Semiconductor Physics, Quantum Electronics & Optoelectronics, 2026. V. 29, No 2. P. 172-179.

Semiconductor physics

Fabrication, structural, and optical properties of ZnO films obtained by pyrolysis of a chelate compound

V.S. Khomchenko*, L.V. Zavyalova, V.V. Strelchuk, O.F. Kolomys, A.S. Nikolenko, O.Yo. Gudymenko, A.A. Korchovyi, V.A. Danko, B.A. Snopok

V. Lashkaryov Institute of Semiconductor Physics, NAS of Ukraine, 41 Nauky Avenue, 03028 Kyiv, Ukraine
**Corresponding author e-mail: khomchenkov@yahoo.com*

Abstract. Thin ZnO films were chemically obtained from two organic compounds. Chelate (or intracomplex) compounds zinc diethyldithiocaramate and zinc acetylacetonate were used as precursors. The effects of precursor type, growth rate, and post-growth annealing of the films were investigated. The microstructure and optical properties of the films were studied and compared using X-ray diffraction (XRD), atomic force microscopy, Raman scattering, and photoluminescence. The XRD results indicated that all the ZnO films had a polycrystalline hexagonal structure and a preferred orientation with the c-axis perpendicular to the substrate. The morphological and optical properties differ markedly for various ZnO films. The reasons of transformation and the nature of optical transitions were discussed. The most intensive UV emission was obtained for the ZnO films grown from zinc acetylacetonate. The ultraviolet/visible emission intensity ratio was 15, comparable to that of epitaxial ZnO films. A simple way for fabricating high-quality ZnO films was presented.

Keywords: ZnO, thin films, metal-organic chemical vapor deposition technique, photoluminescence, atomic force microscopy, X-ray diffraction, Raman spectroscopy.

https://doi.org/10.15407/spqeo29.02.172
PACS 61.05.cp, 68.37.Ps, 78.30.Jw 78.55.Kz, 82.30.Lp

Manuscript received 01.12.25; revised version received 20.04.26; accepted for publication 10.06.26; published online 23.06.26.

1. Introduction

ZnO is a highly attractive material for a wide range of applications in both optical and biological technologies, including display systems [1–4]. Its use in optoelectronic devices arises from a combination of exceptional optical, mechanical, and piezoelectric properties, along with remarkable mechanical and chemical stability [1]. For example, ZnO films are used as transparent electrodes, liquid crystal displays, light-emitting diodes, solar cells, nanolasers, electrical generators, and biosensors [5–10]. Various synthesis techniques have been developed to obtain ZnO films with tailored structural and functional characteristics [2]. However, these techniques typically require use of complex and expensive equipment. Therefore, an important task is to identify and develop alternative approaches that would be simpler, more cost-effective, and still capable of producing high-quality ZnO films. Metal-organic chemical vapor deposition (MOCVD) is well known for enabling fabrication of high-quality films of various materials. Among them, pyrolysis of chelated sulfur-containing metal-organic compounds has been employed to synthesize metal sulfide films [11]. This method has also been successfully adapted for preparing ZnO films [12, 13].

Studies of structural, optical and piezoelectric properties of these films have demonstrated strong potential of the films for use in various optoelectronic, piezoelectric, and acousto-electric devices [14–16]. It was shown that ZnO films exhibit a high degree of structural ordering in the oxygen anion sublattice [15]. At the same time, it is found that the zinc cation sublattice is structurally less perfect and contains point defects responsible for nonradiative recombination. There are also intrinsic point defects that cause visible emission comparable in intensity to the ultraviolet (UV) emission. The UV emission origins from crystalline ZnO, while the visible (VS) emission comes from defects [2]. This indicates that the quality of such films is slightly lower than that of highly perfect ZnO films grown by molecular-beam epitaxy (MBE) [15]. The quality of the ZnO films can be improved by eliminating such defects that require improvements in their growth technology. With this objective, the effects of precursor type, growth rate, and post–growth annealing on the properties of the films was investigated. The quality and degree of structural imperfection of ZnO films were explored using X-ray diffraction (XRD), atomic force microscopy (AFM), Raman spectroscopy, and photoluminescence (PL) measurements.

2. Experimental section

Zinc-oxide films were produced by metal-organic chemical vapor deposition technique [11]. The films were deposited by sputtering 0.1 M of organic zinc salts onto heated (300 °C) silicon and glassy substrates in a quasi-closed volume in air [11]. One of two starting materials was used: zinc diethyldithiocaramate (DD) or zinc acetylacetonate (AA). The film thickness was 0.5 μm. The growth rates of the films were 30 and 50 nm/min. The name of the sample involved the type of precursor and the film growth rate such as ZnO-DD-30, ZnO-DD-50, or ZnO-AA-50. The ZnO-DD and ZnO-AA films were annealed at T_{an} = 600 °C for 2 h at atmospheric pressure in ambient air. For comparison, we used a ZnO film deposited by MBE on a sapphire substrate in vacuum at 510 °C [15].

X-ray diffraction measurements were performed using a DRON-3M X-ray diffractometer under CuK_α irradiation (λ = 0.1541 nm). The film morphological properties were studied with a NanoScope IIIa Dimension 3000 atomic force microscope. To provide high lateral resolution and sensitivity, the tapping mode of the measurements was employed. The measurements were performed using commercial silicon tips (NSG-11, NT-MDT) with a nominal tip apex radius of 10 nm.

Micro-Raman and micro-PL spectra were measured at T = 300 K using a Horiba Jobin Yvon T64000 spectrometer equipped with a confocal microscope and an automated piezo-driven XYZ stage. Discrete lines of an Ar-Kr ion laser (λ_{exc} = 488.0) and He-Cd laser (λ_{exc} = 325.0 nm) with power on the sample surface of 1-2 mW were used for excitation. The laser beam was focused onto the sample to a spot of 0.2 to 0.5 μm in diameter. Spatial mapping of the Raman spectra was realized by displacing the automated stage with a spatial step of 0.1 μm. All the measurements were performed at room temperature.

3. Results and discussion

XRD patterns of all the ZnO films are characterized by the presence of nanocrystallites (NCs) with (100), (002), (101), (102), (110), (103), and (112) orientations. A typical pattern of a ZnO film on silicon substrate is shown in Fig. 1. The seven diffraction peaks match well with the (100), (002), (101), (110), (103), and (112) reflections of the hexagonal wurtzite structure of ZnO, respectively (JCPDS File NO.75-0576 from ASTM). The same structure is observed for the ZnO films on both glass and silicon substrates. The (002) peak at 2θ = 34.41° is the most intense. The intensities of other reflections are insignificant, indicating that the ZnO films are preferentially oriented with the c-axis perpendicular to the substrate. The position of the (002) peak is consistent with that of the ZnO crystal (34.43°). Nevertheless, the half-width of the reflection is sufficiently large (0.4°). This value points to relatively small areas of coherent scattering. The computed average crystallite size is 25 nm.

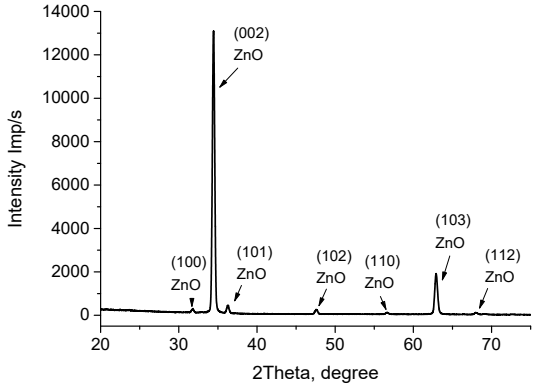

Fig. 1. XRD pattern of the ZnO-AA-50 film on silicon substrate.

Comparative analysis of the XRD patterns of all the ZnO films revealed no differences in the peak positions or full widths at half maxima (FWHM) across the entire diffraction spectrum or across all the sample types. At the same time, the morphological properties of different ZnO films differ markedly. The surface morphology modification caused by changes in the film growth rate was investigated using AFM. The surface images of different ZnO films are presented in Fig. 2. The AFM investigations show that the surface of the ZnO films has a complex nanogranular structure, and the average grain size depends on the film growth rate. The surfaces of the ZnO films demonstrate grain growth and grain aggregation for both growth rates. The surface morphology noticeably changes with a change in the growth rate. The smallest grains (diameters of 150 to 200 nm) aggregate into elongated clusters. The individual grains have a faceted shape. In general, NCs are characterized by a rhomboidal shape. Therefore, we used their average width and length for size characterization.

The difference between the highest and the lowest points within the given area is 200 and 70 nm for the samples DD-30 and DD-50, respectively. From a statistical point of view, the surface transformation at the change in the growth rate can be illustrated using height histograms. The height distributions for the DD-30 (curve *1*) and DD-50 (curve *2*) films are shown in Fig. 2c. Increase in the growth rate promotes grain growth and modifies grain size distribution. Heterogeneity of the distribution and increase in the grain size are observed. The surface height significantly widens for the DD-50 films. Corresponding RMS values are equal to 70 and 48 nm for 30 and 50 nm/min growth rates of films. The root mean square (RMS) roughness of the ZnO-AA film is 44 nm, and the RMS roughness of the ZnO-MBE film is 10 nm. The MBE-ZnO film exhibits a close-packed nanograin hexagonal crystal phase with the grain sizes reaching 140 nm [15]. The ZnO-AA film has a fine-grained morphology and an average grain diameter of 200 nm. Thermal annealing does not change the morphological properties of the ZnO films.

Using confocal Raman spectroscopy [17], a non-destructive analysis of the ZnO film along the growth direction of the structure with submicron resolution was performed.

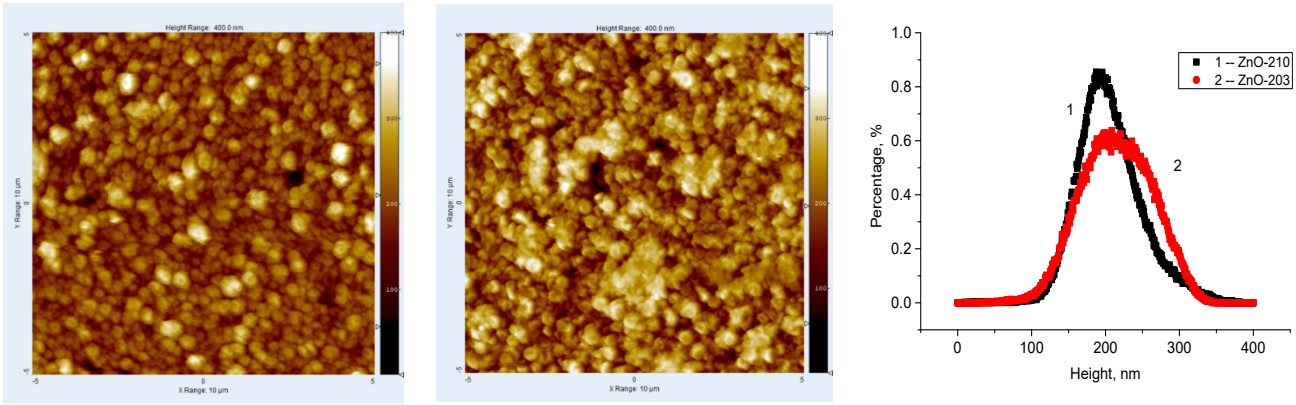

Fig. 2. AFM images of the ZnO-DD-30(left) (a) and ZnO-DD-50 (center) (b) films. Surface height histograms (c) for the ZnO-DD-30 (black, *1*) and ZnO-DD-50 (red, *2*) films.

Raman spectra of the ZnO-DD-30 and ZnO-DD-50 films ranging from 90 to 700 cm^{-1} were obtained, as shown in Fig. 3. The E_2 (low) mode is predominantly associated with nonpolar vibrations of heavier Zn-atoms, while the E_2 (high) mode is associated with displacement of lighter O-atoms. Group theory predicts nine optical phonon branches at the Γ point of the Brillouin zone, $A_1 + 2B_1 + E_1 + 2E_2$, of which the doubly degenerate branch E_1 and the totally symmetric branch A_1 are active in both Raman and infrared spectra [18].

In the Raman spectrum of the sample ZnO-DD-50, the intensive E_2 (low) phonon mode at 98.5 cm^{-1} (Γ = 3.9 cm^{-1}) and E_2 (high) phonon mode at 436.6 cm^{-1} (Γ = 8.4 cm^{-1}) are observed, which indicates satisfactory crystal quality. For the sample ZnO-DD-30, the E_2 (low) phonon mode at 98.3 cm^{-1} (Γ = 4.2 cm^{-1}) and E_2 (high) phonon mode at 436.5 cm^{-1} (Γ = 8.1 cm^{-1}) are also registered. The position of the E_2 (high) band of both ZnO films is shifted by 0.4…0.5 cm^{-1} toward low-frequencies compared to that for an unstrained (bulk) ZnO crystal (437.0 cm^{-1}), while the E_2 (low) band is shifted in the high-frequency region that corresponds to the presence of elastic tensile strain in the growth plane of the film due to the presence of defects in the microstructure and differences in the lattice constants of the ZnO and the substrate.

The bands at 381 and 412 cm^{-1} are assigned to the transverse-optical mode with A_1 (TO) and the first-order transverse-optical mode with E_1 (TO), respectively. The band at 331 cm^{-1} is believed to be second-order Raman scattering phonons E_2 (high) – E_2 (low)(M).

Furthermore, the Raman spectra of the ZnO-DD-50 and ZnO-DD-30 films exhibit a prominent band at ~573 cm^{-1} corresponding to the A_1 (LO) mode. The Raman scattering cross-section of the LO phonon modes in the polar ZnO structure is determined by both the optical deformation potential and the Fröhlich electron-phonon interaction [19]. The above-mentioned A_1 (LO) peak is associated with intrinsic defects [20] and appears more pronounced in the ZnO-DD-30 sample, suggesting different defect states in the ZnO films [21]. Structural defects in the crystal lattice that arise in the initial ZnO matrix during growth induce structural disorder, breaking translational symmetry of allowed phonons and altering the shape and intensity of the Raman bands [22]. The wide band around 500 cm^{-1} is related to the glass substrate. Moreover, the second-order Raman band at 653 cm^{-1}, which arises from a multi-phonon process such as TA+LO (L,H), is observed for the ZnO-DD-30 sample [23].

To determine the strain distribution in the ZnO films, we employed an in-depth scanning approach using non-destructive confocal Raman microspectroscopy. The lateral resolution of this method, defined by the Rayleigh criterion, is $d = 0.61\lambda_{exc}/\mathrm{NA} \approx 330$ nm at an excitation wavelength $\lambda_{exc} = 488.0$ nm, while the axial resolution is $L = 0.89\lambda_{exc}/\mathrm{NA}^2 \approx 0.53$ µm [17], where NA = 0.90 is the numerical aperture of the microscope objective. Confocal Raman spectra of the ZnO-DD-50 film obtained by stepwise focusing of the laser excitation from the surface to the substrate of the sample in the direction perpendicular to the (100) plane with a step of 100 nm are shown in Fig. 4. When the position of the focusing point along the depth of the sample, *i.e.* the excitation depth,

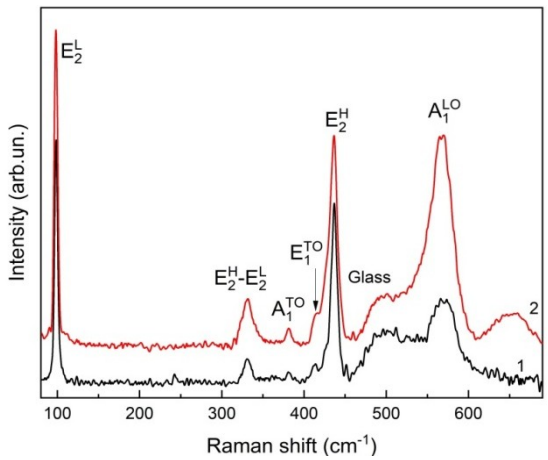

Fig. 3. Micro-Raman spectra of the ZnO-DD-50 (*1*) and ZnO-DD-30 (*2*) films. $E_{exc} = 2.54$ eV. $T = 300$ K.

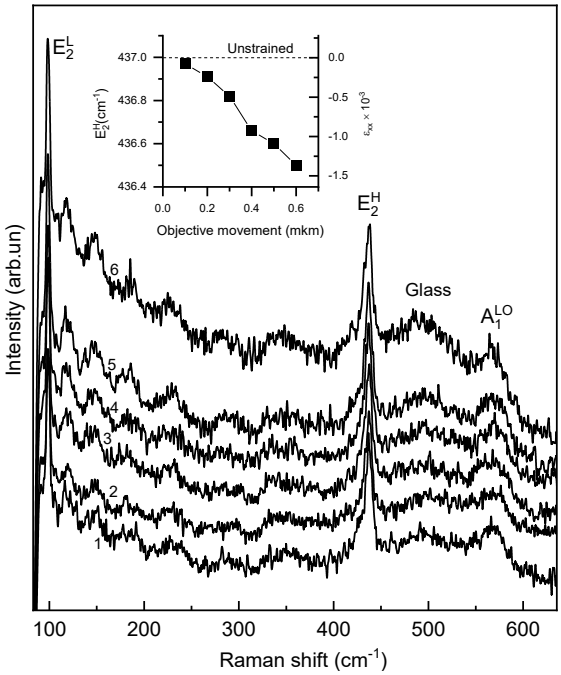

Fig. 4. Selected confocal Raman spectra of the ZnO-DD-50 film obtained by stepwise focusing of laser radiation from the sample surface to the substrate.

is changed, a shift in the frequency position and half-width of the phonon lines from the ZnO structure is observed in the micro-Raman spectra. This indicates a change in the defect-impurity and deformation states of the film throughout its depth. The fact that the frequency of the phonon mode gradually decreases suggests a decrease in elastic tensile deformations when scanning along the growth direction of the ZnO film from the substrate to the surface of the structure. The effect of strain relaxation along the depth of the ZnO epitaxial layers can be due to a decrease in the density of dislocations and/or their inclination. The intensity of the band at 500 cm^{-1} markedly decreases at increasing the distance from the substrate, indicating that it is due to the glass substrate.

The micro-Raman spectra of the ZnO-AA-50 films are noticeably different from those of the ZnO-DD-50 films. The micro-Raman spectra of the different ZnO-AA (*1*, *2*) and ZnO-MBE (*3*) films are shown in Fig. 5. As can be seen from this figure, there is no intense band of complex shape in the 480…560 cm^{-1} region. Two small bands at 500 and 573 cm^{-1} are observed. Since the main contribution to the intensity of the bands at 500 cm^{-1} is due to the glass substrate, we may conclude that the ZnO-AA films are much less porous than the ZnO-DD films. A weak intensity of the 573 cm^{-1} peak is a characteristic feature of perfect wurtzite ZnO films. For example, this peak is very small in the micro-Raman spectrum of the high-quality ZnO MBE film (see Fig. 5). A more detailed comparison of the Raman spectra of the ZnO-AA and ZnO-MBE films is presented in [15]. The MBE ZnO film presents a close-packed nanograin hexagonal crystal phase. It follows from this that the ZnO-AA film has a better crystal structure than the ZnO-DD film.

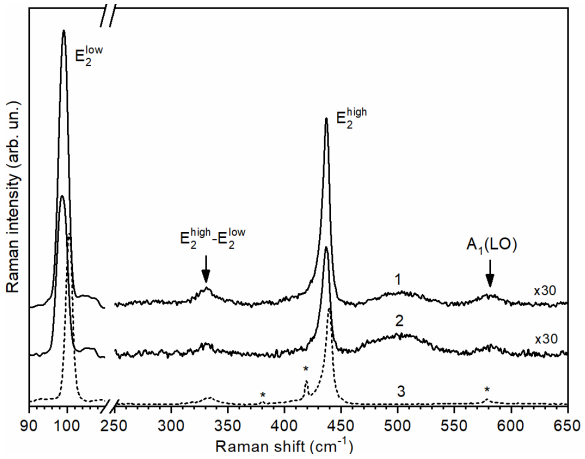

Fig. 5. Micro-Raman spectra of the ZnO-AA-50 (*1*, *2*) and ZnO-MBE (*3*) films. *1* – as-deposited, *2* – after annealing, E_{exc} = 2.54 eV. T = 300 K.

The micro-Raman spectra of the ZnO-DD and ZnO-AA films remain unchanged after thermal annealing (Fig. 5). The PL spectra of the ZnO-DD films grown at different rates are shown in Fig. 6. The PL spectrum of each film was normalized to the maximal intensity value. Both spectra of the ZnO films exhibit two kinds of emission: UV at 377 nm and visible emission with a peak at 500…517 nm. The FWHM (85 meV) and the band position of the UV emission (377 nm) for the ZnO-DD-50 and ZnO-DD-30 films are practically the same, but the intensities greatly differ. The ratio of the UV/VS intensities for the ZnO-DD-50 and ZnO-DD-30 samples is 0.1 and 1.09, respectively. The emission at 377 nm is due to near band edge (NBE) transitions including bound excitons and shallow states [2]. Quenching of the NBE emission can be caused by loss of photogenerated carriers through non-radiative transitions to defect levels.

Wide band emission in the visible spectral region corresponds to radiative transitions from defect states within the bandgap [3]. Gaussian deconvolution of the VS band of the sample ZnO-DD-50 is shown in Fig. 6. Four bands (dash-dots lines) at 480, 520, 572 and 657 nm labeled as D1-D4, respectively, were obtained. For the ZnO-DD-30 films, the same four components: blue, green, yellow, and red, were obtained but with other intensity relationships. In both spectra, the green band has the highest intensity. The difference between the PL spectra of the ZnO-DD-50 and ZnO-DD-30 films is due to the difference in the intensity ratios of the constituent bands. Similar emission bands were observed by other researchers [2, 24–26].

The most significant number of reports refer to the green emission band of ZnO films [2]. The blue, yellow, and red bands were observed in [24–26], respectively. Presence of such bands in the emission spectrum allows us to assume that the ZnO films contain point defects such as oxygen and zinc vacancies and interstitial atoms. The basis for such an assumption is the conclusions about the nature of the luminescence centers made by the authors of the cited above works. At the same time, it is well known that the type of luminescence centers is determined

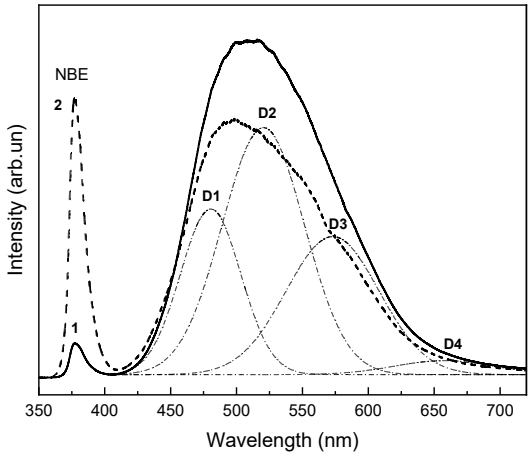

Fig. 6. PL spectra of ZnO-DD-50 (*1*) and ZnO-DD-30 (*2*) films. E_{exc} = 3.81 eV. T = 300 K. The dashed lines show the results of Gaussian multipeak fitting of the VS band of the ZnO-DD-50 film.

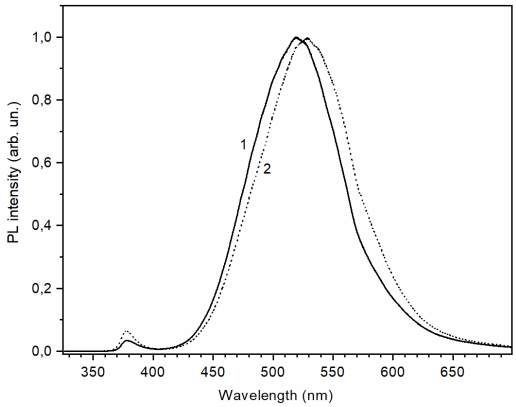

Fig. 7. PL spectra of ZnO-DD-50 films (*1*, *2*). *1* – as-deposited, *2* – after annealing, E_{exc} = 2.54 eV. T = 300 K.

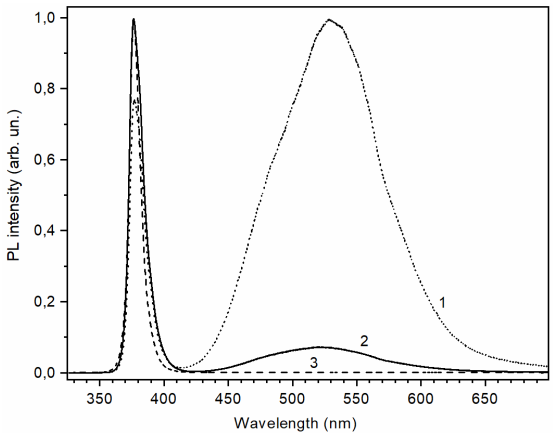

Fig. 8. PL spectra of ZnO-AA-50 (*1*, *2*) and ZnO-MBE (*3*) films. *1* – as-deposited, *2* – after annealing, E_{exc} = 2.54 eV. T = 300 K.

by the conditions of film formation. Our technological process is substantially different from that used by the authors of the above works. Specific details about the nature of the luminescence centers in the ZnO-DD and ZnO-AA films can be identified by examining how different process parameters influence the composition of their spectra. To achieve this, we carried out thermal annealing of the films in air. We found that the nature of the effect of such annealing is the same for the films grown at different rates. Thermal annealing in ambient air leads to suppression of the VS band and enhancement of the UV band. The effect of annealing on the emission spectrum of the ZnO-DD-50 film is shown in Fig. 7. As can be seen from this figure, the wavelength of the maximum UV band does not change, while the VS band maximum for the annealed films shifts toward longer wavelengths from 517 to 527 nm. The VS band intensity decreases by 1.6 times. The UV band intensity does not change, hence, the ratio of the UV/VS intensities respectively increases.

We found that the precursor in the mixture has a significant effect on the emission spectrum of the films. The PL spectra of the ZnO-AA-50 (*1*, *2*) films are shown in Fig. 8. The PL spectrum of the ZnO-MBE film (*3*) is presented for comparison. The spectra were normalized to fit into a single figure. The PL spectrum of the ZnO-AA-50 film consists of two bands, just like the spectrum of the ZnO-DD-50 film. The maximum of the UV band is the same, but the ratio of the UV/VS intensities (0.77) and the VS band maximum (at 530 nm) differ from those for the ZnO-DD-50 film. There is a significant difference in the effect of annealing on the emission spectrum of the ZnO-AA film.

As can be seen from Fig. 8, the PL spectra of as-deposited (*1*) and annealed (*2*) ZnO-AA-50 films are significantly different. The VS band maximum of the annealed films shifts to shorter wavelengths from 531 to 521 nm. The VS PL band intensity decreases by 5 times during oxidation by thermal annealing in ambient air at 600 °C. The UV PL band intensity increases by 3-5 times. The intensity ratio (UV/VS) for the ZnO-AA-50 (as-deposited) and ZnO-AA-50 (annealed) samples is 0.77 and 14, respectively.

The UV emission is from crystalline ZnO and the VS emission is from defects [2]. Therefore, the intensity ratio (UV/VS) is a good indicator of the film quality. Such data indicate a decrease in the number of defects in the films and approaching the properties of the high-quality ZnO-MBE films. The PL spectra of the ZnO-MBE films show no radiation in the VS region.

The difference in the annealing effect on the PL spectra indicates that the emission centers in the ZnO-AA and ZnO-DD films are different. Formation of luminescence centers depends on the type of precursor. This is evidenced by the difference in the emission spectra of the ZnO films grown at the same rate of 50 nm/min (see curves *1* in Figs. 7 and 8). The difference between the emission centers of these films is confirmed by the difference in how storage time affects the PL spectra of the films. The PL spectra of the ZnO-AA films did not change during 12 years, whereas the spectra of the ZnO-DD films changed a lot. Namely, in the latter case, the UV band disappeared or decreased by a factor of 10 and the VS band shifted from 505 to 530 nm regardless of the growth rate.

As shown earlier, the intensity of the VS emission is determined by the green band. Green band emission in ZnO is usually attributed to oxygen or zinc vacancies [2]. A decrease in the intensity of the VS emission after annealing in air (21% oxygen) indicates presence of luminescence centers associated with oxygen vacancies. The quality of such centers is determined form the degree of the decrease of the VS emission intensity. Consequently, the emission from ZnO-AA films is mainly due to oxygen vacancies, whereas in the ZnO-DD films, they constitute only a part of the luminescence centers. Analysis of the obtained information allows us to determine a technological process necessary to produce films with a required composition of the PL spectrum. A one-step process using a DD precursor can be recommended for obtaining films with a green glow. A two-step process using an AA precursor should be used to produce films with UV emission. Formation of intense monochrome UV emission is facilitated by the high-quality structure of the AA films, as evidenced by the corresponding Raman spectra.

Our studies have shown that thermal annealing in air at 600 °C significantly alters the PL spectra but has virtually no effect on the Raman spectra. The difference in the effect of thermal annealing on the micro-Raman and PL spectra indicates different surface defect structures and volumes of the studied films. PL is excited by high-energy light in the region of strong absorption of the ZnO film, while micro-Raman spectra are studied using excitation by relatively low-energy light in *the transparency region of the ZnO films.* Calculations show that a 0.06-μm thick layer is studied with PL method, while practically the entire film volume (0.5 μm) is studied with micro-Raman technique.

4. Conclusions

The results of studies of structural and optical properties of ZnO films obtained by nonvacuum chemical (MOCVD) and molecular-beam epitaxial (MBE) methods are presented. The ZnO MOCVD films were produced by pyrolysis of organometallic compounds. Two types of precursors, namely zinc diethyldithiocaramate and zinc acetylacetonate, were used. The crystal structure, surface topology, phonon, and emission properties of the ZnO MOCVD films were studied. The effects of growth rate, precursor type, and post-growth annealing on the films were investigated. It was found that the amount and types of defects depend on the precursor type, film growth rate, and thermal annealing conditions. For all the ZnO films, increase of the UV emission as well as suppression of the wide bands in the VS region of the PL spectra as a result of thermal annealing were observed. The most intensive UV emission was obtained for the ZnO films grown from zinc acetylacetonate. The UV/VS emission intensity ratio was 15, comparable to that for epitaxial ZnO films. The data imply high-quality of the ZnO films obtained by simple pyrolysis of chelated sulfur-containing metal-organic compounds.

References

1. Klingshirn C. ZnO: From basics towards applications. *phys. status solidi (b)*. 2007. **244**, No 9. P. 3027–3073. https://doi.org/10.1002/pssb.200743072.
2. Özgür Ü., Alivov Y.I., Liu C. *et al.* A comprehensive review of ZnO materials and devices. *J. Appl. Phys*. 2005. **98**, No 4. P. 041301. https://doi.org/10.1063/1.1992666.
3. Saravade V., Feng Z.C., Nafisa M.T. *et al.* Advances in growth, doping, and devices and applications of zinc oxide. *J. Vac. Sci. Technol. A*. 2024. **42**. P. 020802. https://doi.org/10.1116/6.000317.
4. Kanagamani K., Muthukrishnan P., Kathiresan A. *et al.* Detoxication and theranostic aspects of biosynthesised zinc oxide nanoparticles for drug delivery. *Acta Metall. Sin. (Engl. Lett.)*. 2021. **34**. P. 729–740. https://doi.org/10.1007/s40195-020-01116-x.
5. Zhang X.M., Lu M.Y., Zhang Y. *et al.* Fabrication of a high-brightness blue-light-emitting diode using a ZnO-nanowire array grown on *p*-GaN thin film. *Adv. Mater*. 2009. **21**. P. 2767–2770. https://doi.org/10.1002/adma.200802686.
6. Ahmed M.A., Coetsee L., Meyer W.E., Nel J.M. Influence (Ce and Sm) co-doping ZnO nanorods on the structural, optical and electrical properties of the fabricated Schottky diode using chemical bath deposition. *J. Alloys Compd*. 2019. **810**. P. 151929. https://doi.org/10.1016/j.jallcom.2019.151929.
7. Pietruszka R., Schifano R., Krajewski T.A. *et al.* Improved efficiency of *n*-ZnO/*p*-Si based photovoltaic cells by band offset engineering. *Sol. Energy Mater. Sol. Cells.* 2016. **147**. P. 164–170. https://doi.org/10.1016/j.solmat. 2015.12.018.
8. Wang Z.L., Song J. Piezoelectric nanogenerators based on zinc oxide nanowire arrays. *Science.* 2006. **312**. P. 242–246. https://doi.org/10.1126/science.1124005.
9. Wang X., Song J., Liu J., Wang Z.L. Direct-current nano-generator driven by ultrasonic waves. *Science*. 2007. **316**, No 5821. P. 102–105. https://doi.org/10.1126/science.1139366.
10. Bagga S., Akhtar J., Mishra S. Synthesis and applications of ZnO nanowire: A review. *AIP Conf. Proc.* 2018. **1989**. P. 020004. https://doi.org/10.1063/1.5047680.
11. Zhanorsky L., Zavyalova L., Svechnikov G. Metal chalcogenide films prepared from chelate organometallic compounds. *Thin Solid Films*. 1985. **128**. P. 241–249. https://doi.org/10.1016/0040-6090(85)90076-8.
12. Khomchenko V.S., Kryshtab T.G., Savin A.K. *et al. Superlattic. Microstruct*. 2007. **42**. P. 94–98. https://doi.org/10.1016/j.spmi.2007.04.016.
13. Khomchenko V., Sopinskyy M., Dan'ko V., Olkhovik G. Doping the thin films by using the original Close Space Sublimation method. *SPQEO*. 2020. **23**. P. 5–28. https://doi.org/10.15407/spqeo23.01.05.
14. Khomchenko V.S., Roshchina N.N., Zav'yalova L.V. *et al.* Structure, emission and piezoelectric properties of MOCVD-grown ZnS,ZnS-ZnO and Zn films. *Tech. Phys*. 2014. **59**. P. 93–101. https://doi.org/10.1134/S1063784214010071.

15. Strelchuk V.V., Avramenko K.A., Romanyuk A.S. *et al.* Structural and optical properties of ZnO films produced by a nonvacuum chemical technique. *Semiconductors*. 2014. **48**, No 9. P. 1145–1150. https://doi.org/10.1134/S106378261409019X.
16. Snopok B.A., Zavyalova L.V., Tatyanenko N.P. *et al.* The effect of small addition of copper on the growth process, structure, surface charge and adsorption properties of ZnO films in the pyrolysis of dithiocarbamates. *J. Mater. Adv*. 2021. **2**. P. 3637–3654. https://doi.org/10.1039/d1ma 00199j.
17. Kim Y., Lee E.J., Roy E.J. *et al.* Measurement of lateral and axial resolution of confocal Raman microscope using dispersed carbon nanotubes and suspended graphene. *Curr. Appl. Phys.* 2020. **20.** P. 71–77. https://doi.org/10.1016/j.cap.2019.10.012.
18. Dash S., Padhan P. Lattice thermal conductivity of ZnO: experimental and theoretical studies. *Phys. Chem. Chem. Phys.* 2024. **26**. P. 14754–14765. https://doi.org/10.1039/D4CP00575A.
19. Liu T.-H., Zhou J., Xu Q. *et al.* Significant suppression of phonon transport in polar semiconductors owing to electron-phonon induced dipole coupling: An effect of breaking centrosymmetry. *Mater. Today Phys.* 2022. **22**. P. 100598. https://doi.org/10.1016/j.mtphys.2021.100598.
20. Lva J., Lib C., Chai Z. Defect luminescence and its mediated physical properties in ZnO. *J. Lumin*. 2019. 208. P. 225–237. https://doi.org/10.1016/j.jlumin.2018.12.050.
21. Pekar G.S., Singaevsky A.F., Kolomys O.F. *et al.* Structural, optical and magnetic properties of stencil-free printed ZnO layers doped with Fe^{2+} and Fe^{3+} ions. *Mater. Chem. Phys*. 2021. **276**. P. 125329. https://doi.org/10.1016/j.matchemphys.2021.125329.
22. Lee J., Kowalik I.A., Arvanitis D. *et al.* Room Temperature Multiferroicity in Bi-Doped ZnO Enabled by Lattice Distortion and Electronic Reconstruction, Small Methods. 2026. P. e70770 https://doi.org/10.1002/smtd.70770.
23. Pekar G.S., Singaevsky G.S., Kolomys O.F. *et al.* Magnetic and optical properties of printed ZnO:Co polycrystalline layers, Mater. Sci. Semicond. Process. 2021. **135**. P. 106054. https://doi.org/10.1016/j.mssp.2021.106054..
24. Ghamsari M.S., Alamdari S., Razzaghi D., Pirlar M.A. ZnO nanocrystals with narrow-band blue emission. *J. Lumin*. 2019. **205**. P. 508–518. https://doi.org/10.1016/j.jlumin.2018.09.064.
25. Panigrahi J., Singh P.K., Gupta G., Vandana. Growth and luminescence characteristics of zinc oxide thin films deposited by ALD technique. *J. Lumin*. 2021. **233**. P. 117797. https://doi.org/10.1016/j.jlumin.2020.117797.
26. Achour A., Islam M., Vizireanu S. *et al.* Orange/red photoluminescence enhancement upon SF_6 plasma treatment of vertically aligned ZnO nanorods. *Nanomaterials*. 2019. **9**, No 5. P. 794. https://doi.org/10.3390/nano9050794.

Authors and CV

V.S. Khomchenko, PhD, Senior Researcher at the V. Lashkaryov Institute of Semiconductor Physics, NASU. Author of more than 200 publications and 3 patents. Research interests: physics and technology of semiconductor materials, light-emitting structures, *etc*.); analysis, diagnostics, modeling and predicting of physical processes in various objects.
http://orcid.org/0000-0001-6127-0037

L.V. Zavyalova, PhD, Senior Researcher at the Institute of Semiconductor Physics, NASU. Authored over 110 publications, 1 monograph, and 12 patents. Her research focuses on development and study of chemical methods for producing films of semiconductor compounds and the properties of the resulting light-emitting and piezoelectric structures based on films of sulfides, oxosulfides, and metal oxides, primarily ZnS and ZnO. E-mail: zavjalov007@gmil.com, http://orcid.org/0000-0002-7771-9035

V.V. Strelchuk, Doctor of Sciences, Professor, Leading Researcher at the Laboratory of Submicron Optical Spectroscopy, V. Lashkaryov Institute of Semiconductor Physics, NASU. Field of researches: physics of semiconductors, Raman and photoluminescence spectroscopy of semiconductors, nanostructures and nanoscale materials. Authored over 300 publications, 10 patents, and 6 textbooks. E-mail: viktor.strelchuk@ccu-semicond.net, https://orcid.org/0000-0002-6894-1742

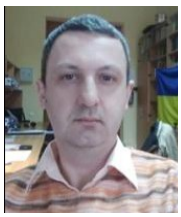

O.F. Kolomys, PhD, Senior Researcher at the Laboratory of Submicron Optical Spectroscopy, V. Lashkaryov Institute of Semiconductor Physics, NASU. Field of research: structural and optical study of semiconductor materials and nanostructures.
Authored over 130 publications, 3 patents, and 3 textbooks. E-mail: olkolomys@gmail.com, https://orcid.org/0000-0002-1902-4075

A.A. Korchovyi, PhD, Senior Researcher at the Laboratory for Scanning Probe Microscopy, V. Lashkaryov Institute of Semiconductor Physics, NASU. Authored over 100 papers. Expertise: atomic force microscopy, semiconductor materials and nanostructures. E-mail: akorchovyi@gmail.com, https://orcid.org/0000-0002-8848-7049

A.S. Nikolenko, PhD, Senior Researcher at the Submicron Optical Spectroscopy Laboratory, V. Lashkaryov Institute of Semiconductor Physics, NASU. Field of research: semiconductor nanostructures and heterostructures, Raman, photoluminescence and FTIR spectroscopy. Authored over 120 publications, 6 patents, and 4 text-books.
E-mail: nikolenko@isp.kiev.ua,
https://orcid.org/0000-0001-6775-3451

V.A. Dan'ko, Doctor of Sciences in Physics and Mathematics, Leading Researcher at the V. Lashkaryov Institute of Semiconductor Physics, NASU. His main research activity is in the field of optics of thin films, photostimulated processes in thin film structures, nanoparticles and nanostructures, and interference lithography. Authored over 170 publications and patents. E-mail: dankova@ukr.net, http://orcid.org/0000-0001-8106-3182

O.Yo. Gudymenko, PhD, Senior Researcher at the Department of Ion-Beam Engineering, V. Lashkaryov Institute of Semiconductor Physics, NASU. Author of more than 60 publications. Field of research: solid-state physics, dynamical theory of diffraction of radia tion, X-ray optics, and X-ray diffraction analysis of semiconductor crystals. Authored over 120 publications.
E-mail: gudymen@ukr.net,
https://orcid.org/0000-0002-5866-8084

B.A. Snopok, Professor, Dr. Habil., Head of the Department of Optoelectronics at the V. Lashkaryov Institute of Semiconductor Physics, NASU. His scientific interests include nanoscale-specific analytics, multivariate "coding" of nanomaterials, bionano composites, nanophysics, plasmonics, biosensors and analytical methods of diagnostics.
E-mail: b_snopok@yahoo.com,
http://orcid.org/0000-0002-0544-2663

Authors' contributions

Khomchenko V.S.: methodology, formal analysis, writing – original draft, writing – review & editing.
Zavyalova L.V.: methodology, data curation, writing – original draft, writing – review & editing.
Strelchuk V.V.: conceptualization, supervision, validation, writing – review & editing.
Kolomys O.F.: investigation, formal analysis.
Nikolenko A.S.: investigation, formal analysis.
Gudymenko O.Yo.: investigation, resources.
Korchovyi A.A.: investigation, data curation.
Danko V.A.: methodology, visualization, writing – original draft.
Snopok B.A.: conceptualization, validation, project administration, supervision.

Виготовлення, структурні та оптичні властивості плівок ZnO, отриманих піролізом хелатної сполуки

В.С. Хомченко, Л.В. Завьялова, В.В. Стрельчук, О.Ф. Коломис, А.С. Ніколенко, О.Й. Гудименко, А.А. Корчовий, В.А. Данько, Б.А. Снопок

Анотація. Тонкі плівки ZnO були отримані хімічним шляхом з двох органічних сполук. Як прекурсори використовувалися хелатні (або внутрішньокомплексні) сполуки: діетилдитіокарамат цинку та ацетилацетонат цинку. Досліджено вплив типу прекурсора, швидкості росту та пост-ростового відпалу плівок. Мікроструктуру та оптичні властивості плівок вивчали та порівнювали за допомогою рентгенівської дифракції (XRD), атомно-силової мікроскопії, комбінаційного розсіювання та фотолюмінесценції. Результати XRD показали, що всі плівки ZnO мають полікристалічну гексагональну структуру та переважну орієнтацію з віссю *c*, перпендикулярною до підкладки. Морфологічні та оптичні властивості різних плівок ZnO суттєво відрізняються. Обговорено причини перетворення та характер оптичних переходів. Найбільш інтенсивне УФ-випромінювання було отримано для плівок ZnO, вирощених з ацетилацетонату цинку. Співвідношення ультрафіолетового/видимого випромінювання становило 15, що можна порівняти з епітаксійними плівками ZnO. Представлено простий спосіб виготовлення високоякісних плівок ZnO.

Ключові слова: ZnO, тонкі плівки, метод металоорганічного хімічного осадження з парової фази, фотолюмінесценція, атомно-силова мікроскопія, рентгенівська дифракція, раманівська спектроскопія.